Journal of Molecular Liquids 367 (2022) 120474

Contents lists available at ScienceDirect

Journal of Molecular Liquids

journal homepage: www.elsevier.com/locate/molliq

Electrolyte adsorption in graphene and hexagonal boron nitride nanochannels

Nasim Anousheh [a,*], Azar Shamloo [b], Seifollah Jalili [c], Jack A. Tuszynski [d,e]

[a] Department of Intelligent Systems Engineering, Indiana University, 700 N. Woodlawn Avenue, Bloomington 47408, IN, USA
[b] Department of Biochemistry, Microbiology, and Bioinformatics, Universite Laval, 2325, rue de l'Universite, Quebec City, G1V 0A6 Quebec, Canada
[c] Department of Chemistry, K.N. Toosi University of Technology, Tehran, Iran
[d] Department of Physics, University of Alberta, 11335 Saskatchewan Dr NW, Edmonton, T6G 2M9, Alberta, Canada
[e] Department of Mechanical and Aerospace Engineering, Polytechnic di Torino, Corso Duca degli Abruzzi, 24, Turin 10129, Italy

ARTICLE INFO

Article history:
Received 14 June 2022
Revised 13 September 2022
Accepted 23 September 2022
Available online 28 September 2022

Keywords:
Graphene
Hexagonal boron nitride
Confined electrolytes
Glide
Shuffle
Molecular dynamics simulation

ABSTRACT

Understanding the dynamics of confined electrolytes through graphene-based channels is essential in multiple fields of science including: (a) developing novel artificial membranes for drug delivery, DNA sequencing and water desalination and (b) developing quantum nanoelectronic devices. In this work, All-Atom molecular dynamics simulations are used to study the adsorption of confined NaCl electrolyte solutions in graphene (GR), hexagonal boron nitride (hBN) and combined GR-hBN-GR nano-channels over a wide range of electrolyte concentrations $c \in (0.1, 2)$ M. The behavior of electrolytes confined between these surfaces is analyzed by evaluating the ionic density profiles, Potential of Mean Force (PMF), net charge density and integrated charge. Although neither graphene nor hBN has net electric charge, we observed significant changes in the ionic structure including the enhanced accumulation of sodium and the depletion in chloride density close to the hBN interfaces at low salt concentration. However, increasing the salt concentration leads to accumulation of chloride close to hBN surfaces. Two different types of hBN-GR junctions are considered in this study: a) shuffle (zigzag bonds) and (b) glide (parallel bonds). High adsorption of sodium and chloride ions near shuffle GR-hBN-GR surfaces is observed due to electrostatic attraction forces between the sodium and nitrogen atoms and between chloride and boron atoms at hBN–graphene junctions across zigzag bonds. This study reveals that GR-hBN-GR with shuffle interface is highly advantageous in adsorbing sodium and chloride ions than graphene and hBN alone. To the best of our knowledge, this is the first study that elucidates the interaction between monovalent electrolytes and GR-hBN-GR heterostructures in a confined medium.

1. Introduction

The unique features of graphene-based nano-channels have brought remarkable opportunities for innovation in the field of water desalination [1], biomedicine [2,3] and biotechnology [4]. Inspired by the unique properties of graphene, the graphene-like materials such as hexagonal boron nitride (hBN) have attracted considerable attention because of their excellent high surface area [5] and high adsorption performance [6]. Recent advances in nanotechnology have led to the generation of the graphene and hBN integrated into a lateral heterostructure [7,8]. Heterostructures of graphene and hBN have high ionic sensitivity that leads to increased transconductance [9]. The nature of this lateral nanoarray heterostructure provides a promising route not only for quantum nanoelectronics innovations due to the higher conductivity [10–12] but also it opens new possibilities for the manipulation of biomolecules in biological media [13,14].

In order to study electrolytes in detail, experimental [9,15–17] and theoretical approaches [18] and computer simulations [19–23] have been created that describe the properties of electrolytes near the graphene-like and graphene-based surfaces. In addition, the graphene-based nanochannel models such as carbon nanotube networks [24], uncharged [25] and charged [26] nanoporous graphene, ozark graphene nanopore [27] and graphite [28] have been proposed to explore the dynamics of ions and water molecules. In theoretical studies, it has been shown that hBN nanotubes (acting as a graphene-like nanochannel) can be promising in exploring ion channels due to relatively strong van der Waals interactions between water molecules and nitrogen atoms [29,30]. Srivastava et al. [31] showed that an hBN nanosheet can be an efficient adsorbent for the cations such as arsenic due to strong electrostatics

* Corresponding author.
E-mail address: nanoushe@iu.edu (N. Anousheh).

https://doi.org/10.1016/j.molliq.2022.120474
0167-7322/

interaction between the sodium ions and hBN surface. Another simulation work [19] showed that Na^+ repelled from the graphene interface because its polarizability is weak and there are no compensating dipole–dipole interactions. On the other hand, Cl^- ions are strongly adsorbed at the uncharged graphene/water interface. Moreover, a recent experimental study has demonstrated the enhanced ionic sensitivity in graphene/hBN heterostructure materials [9]. Not only the dynamics of the ions but also the dynamics of the water have been affected by these surfaces [32–36]. Poggioli and Limmer [35] used molecular dynamics simulations to show that the hydrogen atoms of water are oriented toward the negatively charged nitrogen centers in the hBN surface. As a result, the hydrogen density and a net electrostatic interaction near the hBN surface increase. It has been shown that the friction coefficient on hBN is three times larger than that of graphene due to its specific electronic structure effects [36]. This leads to hBN sheets adsorbing water more than graphene sheets which makes it suitable for the future design of membranes. These and other previous studies [26,30,37] have shown that the water and ionic adsorptions on hBN differ from graphene and are strongly affected by the surface material of the channel.

Nonetheless, little is known about the structure and dynamics of confined electrolytes in molecular detail at heterostructures of graphene-hBN surfaces. Moreover, the structure imperfections at graphene-hBN interfaces have been the greatest challenge [38–40] and the quality of the hBN and graphene interfaces, is critical for the high device performance of the in-plane.

The aim of this work is to provide insights into the adsorption and separation of NaCl electrolyte over a wide range of concentrations $c \in (0.1, 2)$ M confined in graphene, hBN and combined GR-hBN-GR nanosheets using All-Atom molecular dynamics (MD). All-Atom MD simulations show great promise in advancing our understanding of the movement behavior of aqueous solutions containing salt ions at various solid/water interfaces [41]. Two different types of hBN-GR interfaces were considered in this work: shuffle and glide corresponding to hBN-GR junction across zigzag bonds and parallel bonds respectively (see Fig. 1). The crucial details concerning the structural behavior of electrolyte confined in these nanochannels were provided which could benefit subsequent experimental work.

2. Models and Methods

The simulation cell is a rectangular box of dimensions $l_x \times l_y \times h$. In the z direction h = 3.4 nm and in both x and y directions $lx = ly$ = 8 nm, which is large enough to obtain a bulk like behavior at the center of the box ($z = 0$). The 2D nanosheets may assemble in paper-like structures with interlayer distance on a nanometer scale and construct nanochannels [42]. It should be noted that the actual nanochannel constructed by 2D materials is very complex due to the different topology patterns and wrinkle surface [43]. In this work we consider the ideal case to simplify the simulations. The system of interest consists of two planar sheets located along the z direction at positions $z = -h/2$ and $z = h/2$ to construct the nanochannels. The simulation box is periodic in x and y axes which produces a slab of electrolyte that is extended along the x and y directions but confined between the two sheets along the z direction. Each sheet has the dimensions of $8 \times 8\ nm^2$. The sheets are 3.4 nm far from each other to form the boundaries of the simulation box along the z direction. Four systems with different planar surfaces are investigated. The first system consists of two graphene sheets. Each graphene sheet contains 2508 carbon atoms. The second system consists of two hBN sheets. Each hBN sheet contains 1254 boron and 1254 nitrogen atoms. The third and fourth systems contain two combined GR-hBN-GR sheets. These two later systems have two different types of in-plane junctions between hBN and graphene corresponding to junction across parallel bonds and across zigzag bonds (see Fig. 1). We call these junctions glide and shuffle respectively, as reported in McHugh et al. [44]. Experimentally, the interatomic spacings in the graphene and hBN lattices are found to be nearly identical (0.142 nm in graphene and 0.145 nm in hBN) and are set to 0.142 nm in the simulations [45,46]. An example of the initial simulated configuration of monovalent electrolyte NaCl confined between two GR-hBN-GR sheets with shuffle interface is shown in Fig. 2. The atoms are visualized and the snapshots were rendered using Furious Atoms software [47,48]. The ionic structure of aqueous NaCl electrolyte solutions confined by these interfaces over a wide range of concentrations $c \in (0.1, 2)$ M was studied. Electrolyte concentration was defined as $c = N/V$, where N is the number of electrolyte cations (Na^+) or anions (Cl^-) and $V = l_x \times l_y \times l_z$ is the volume of the simulation box [49]. For all systems, depending on the electrolyte concentration, the number of water molecules in the main simulation cell varied between 5163 to 5603. Water molecules were simulated using an extended simple point charge (SPC/E) model since it is less computationally demanding [50]. SPC/E is an effective rigid three-site pair potential model having both Lennard-Jones (LJ) and Coulombic components. The three interaction sites correspond to the three atoms of a water molecule. Each atom was given a point charge to include electrostatic interactions with q_O = −0.8476 e and q_H = 0.4238 e. Sodium ions and chloride ions were assigned with charges of q_{Na} = 1.0 e and q_{Cl} = −1.0 e respectively. The partial charges used for nitrogen, boron and carbon atoms were q_N = −0.4 e, q_B = 0.4 e and zero respectively. To neutralize the local charge at the edges between hBN and graphene, the carbon atom that forms a covalent bond with a boron atom has been assigned a charge of −0.133 e, and the carbon atom that forms a covalent bond with a nitrogen atom has been assigned a charge of 0.133 e [51]. The Hamiltonian of the confined electrolyte system is the sum of the total steric and electrostatic energies associated with ion-ion interactions and the

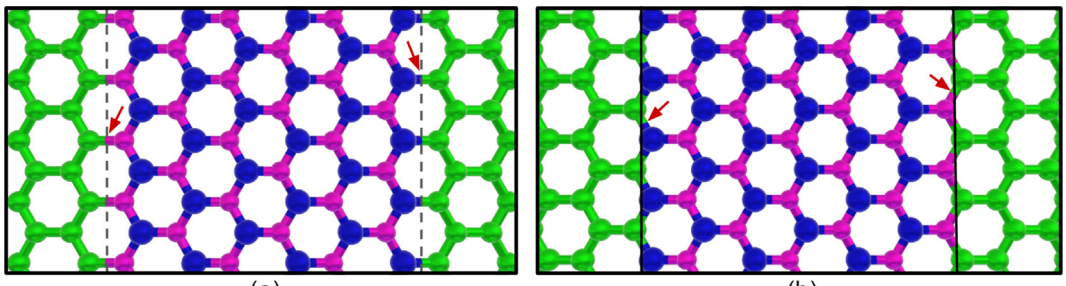

Fig. 1. Illustrations of two different types of in-plane junctions between hBN and graphene: (a) glide junction across the parallel bonds (black dash line) and (b) shuffle junction across the zigzag bonds (solid black line). Carbon, boron and nitrogen atoms in the 2D material are colored in green, purple and blue respectively. (For interpretation of the references to colour in this figure legend, the reader is referred to the web version of this article.)

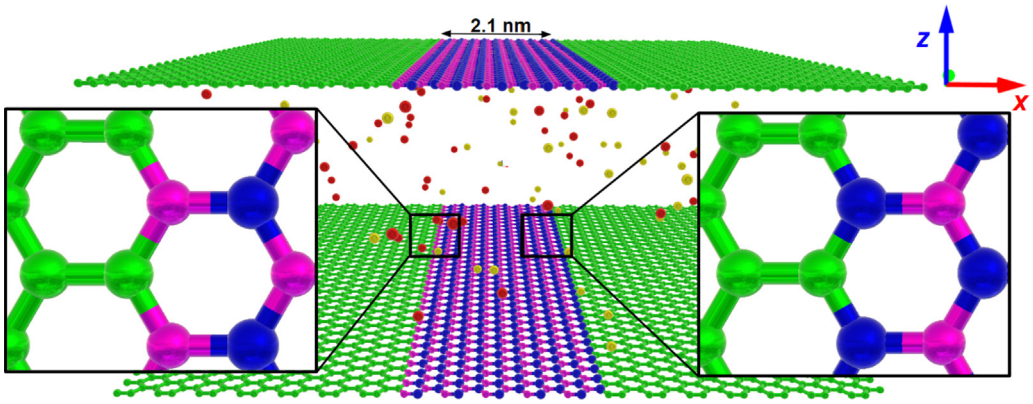

Fig. 2. The simulated configuration of monovalent electrolyte NaCl is confined between two GR-hBN-GR sheets. The interface between hBN and graphene is along zigzag bonds (shuffle). The area of the hBN ribbon is $2.1 \times 8\ nm^2$. Carbon, boron and nitrogen atoms in the 2D material are colored in green, purple and blue respectively. Na^+ and Cl^- ions are colored in red and yellow respectively. Water molecules are not shown for visual clarity. (For interpretation of the references to colour in this figure legend, the reader is referred to the web version of this article.)

interaction between the ions and the two planar sheets. Ion-ion and ion-interfaces steric interactions were modeled using the standard purely-repulsive and shifted Lennard-Jones (LJ) potential [52]. For a pair of ions separated by distance r, this potential is:

$$\frac{U_{LJ}}{k_B T} = 1 + 4\left[\left(\frac{\sigma}{r}\right)^{12} - \left(\frac{\sigma}{r}\right)^{6}\right], \tag{1}$$

for $r \leqslant 2^{1/6}\sigma$, where, σ is the average diameter of the two ions, k_B is the Boltzmann constant and T is the temperature. For $r > 2^{1/6}\sigma, U_{LJ} = 0$. Lennard-Jones parameters for heteroatomic interactions are determined using Lorentz-Berthelot mixing rules. The Lennard-Jones parameters used in this work are provided in Table 1.

The MD simulations have been carried out using LAMMPS [53]. All simulations were executed in the NVT ensemble at a temperature of $T = 298$ K that is maintained using a Nose–Hoover thermostat [54]. The non-electrostatic interactions were computed by direct summation with a cut-off length of 1.2 *nm*. The electrostatic interactions were computed using the Particle Mesh Ewald (PME) method [55]. Each system was simulated for 5 *ns* to reach equilibrium with a timestep of 1 femtosecond. After equilibrium, the systems were simulated for another 80 *ns* and trajectory data for computing ionic distributions were collected every 0.1 *ps*. The nanosheets were fixed at their initial lattice positions while the electrolyte solution moved freely. The density distribution in the direction perpendicular to the sheets (the direction z) and along the sheets (the direction x) for cations, anions and water was obtained from the MD trajectories. For the density in the z and x directions, the computational domain was divided into slab bins in the z and x directions respectively. The bin size of 0.05 *nm* was chosen to ensure that the data are collected properly. Once the density profiles were obtained, the charge density and the integrated charge distribution were calculated. The integrated charge describes the overall charge close to the surface. The procedure to get the integrated charge is detailed in [56,57]. The integrated charge is represented using the following equation:

$$S(z) = \sigma_s + \int_{-h/2}^{z} \rho(z\prime)dz\prime \tag{2}$$

Where z is the normal distance from sheet ($z = 0$ is located on the sheet). $S(z)$ is defined for $-h/2 \leqslant z \leqslant 0$, i.e., up to the center of the confined region. σ_s is the surface charge density. Since graphene, hBN and GR-hBN-GR sheets do not have net electric charge, σ_s is zero. ρ is the charge density given by:

$$\rho(z) = en_+(z) - en_-(z) \tag{3}$$

Where e is the electronic charge, and $n_+(z)$ and $n_-(z)$ are the number density profiles of sodium and chloride ions respectively. We further probed the energetic properties of Na^+ and Cl^- ions across theses channels (z-axis) by calculating the potential of mean force (PMF) [58]:

$$E_{PMF} = -k_B T\left(ln\frac{n_\alpha(z)}{\overline{n}(0)}\right) \tag{4}$$

Where k_B is Boltzmann constant, T is the temperature, $n(z)$ is the number density ($\alpha = Na^+, Cl^-$) along the z direction and $\overline{n}(0)$ is the bulk number density.

Table 1
Interaction parameters for the potential models used in this work. The parameters are taken from [26].

Interaction	ϵ (eV)	σ (nm)
H–H	0	0
O–O	0.006736616	0.31656
O–Na	0.002079272	0.28704
O–Cl	0.005575083	0.38068
O–C	0.004062790	0.31900
Na–Na	0.000641772	0.25752
Na–Cl	0.001702700	0.35116
Na–C	0.001350014	0.29876
Cl–C	0.003619748	0.39240
Cl–Cl	0.004613823	0.44480
B–O	0.005264404	0.33100
B–Na	0.001617408	0.30141
B–Cl	0.004336703	0.39505
N–O	0.006504617	0.32660
N–Na	0.002001874	0.29558
N–Cl	0.005367560	0.39065

3. Results

3.1. Density profiles

We first discuss the density profiles of Na^+ and Cl^- ions confined in graphene (Fig. 3), hBN (Fig. 4) and GR-hBN-GR nanosheets with glide (Fig. 5) and shuffle interfaces (Fig. 6). Profiles are shown for different electrolyte concentrations in the range $c \in (0.1, 2)$ M. From Fig. 3, the layering of both Cl^- and Na^+ ions between the channel walls are seen. There is no significant ion absorption near the surfaces. Since the graphene surface is uncharged, the presence of excluded-volume interactions can mainly lead to layering effects

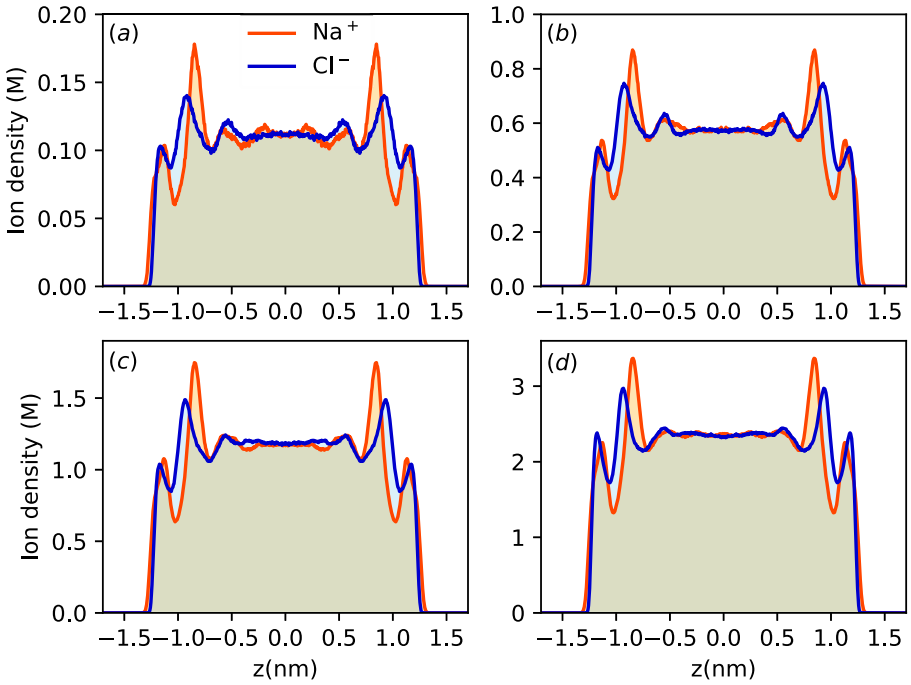

Fig. 3. Density profiles of $n_+(z)$ of sodium (orange) and $n_-(z)$ of chloride (blue) confined within two parallel homogeneous graphene sheets. Results are shown for different electrolyte concentrations: (a) 0.1 M, (b) 0.5 M, (c) 1.0 M, (d) 2.0 M. For all the systems, two surfaces are located at $z = -h/2$ and $z = h/2$ where $h = 3.4$ *nm*. (For interpretation of the references to colour in this figure legend, the reader is referred to the web version of this article.)

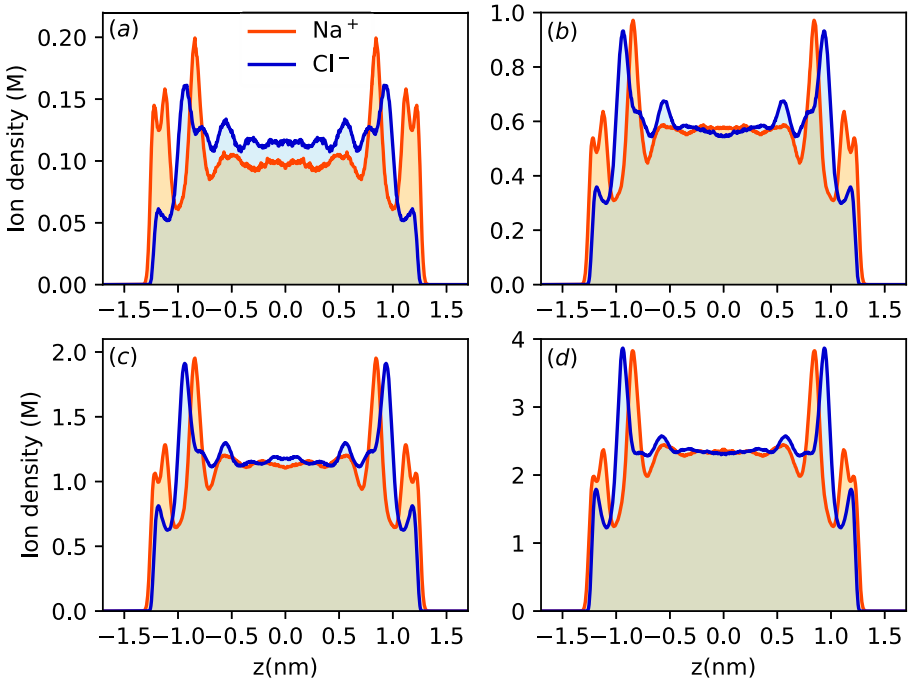

Fig. 4. Density profile $n_+(z)$ of sodium (orange) and $n_-(z)$ of chloride (blue) confined within two parallel homogeneous hBN sheets. Results are shown for different electrolyte concentrations: (a) 0.1 M, (b) 0.5 M, (c) 1.0 M, (d) 2 M. For all the systems, two surfaces are located at $z = -h/2$ and $z = h/2$ where $h = 3.4$ *nm*.

near the surfaces. In all cases, the first peak values of Na^+ and Cl^- ions are close to the value of the bulk ion concentration. An accumulation of the Na^+ ions is observed at the second layer near the neutral graphene surface with respect to the bulk. As the salt concentration increased, the locations of accumulation layers for Na^+ and Cl^- ions remained stable, but their peak values increased. Increasing salt concentration from 0.1*M* to 2*M* does not impact the layering organization of the ion density. This finding suggests that a confinement effect is the main ingredient of the layering structure near the uncharged graphene surfaces.

Density profiles of electrolyte confined in hBN sheets (see Fig. 4) show significant changes in the ionic structure including the enhanced accumulation of Na^+ ions in the first layer near the hBN sheet while Cl^- ions are depleted from the surface. At low salt

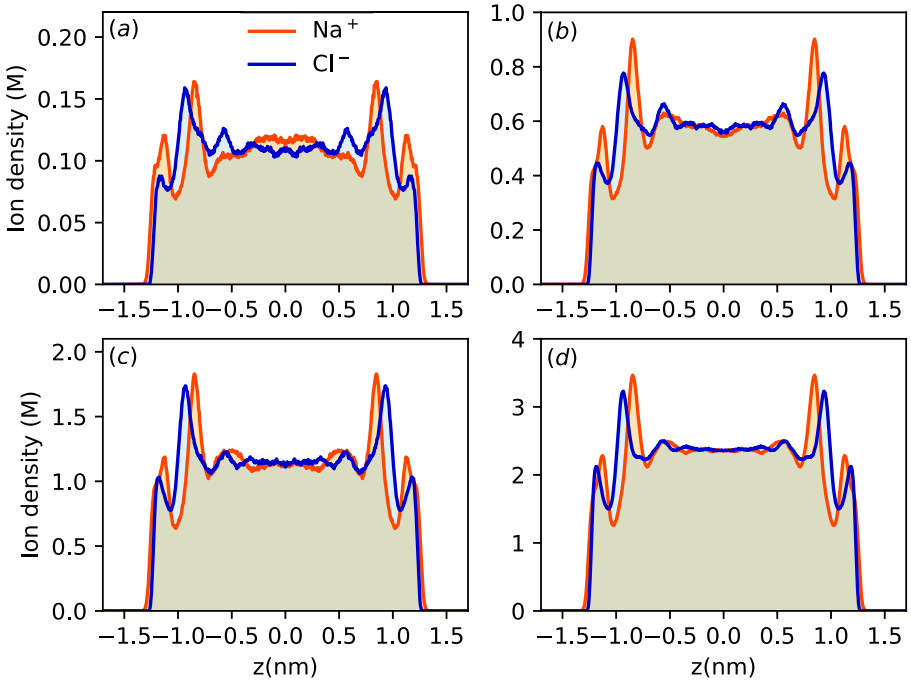

Fig. 5. Density profiles of $n_+(z)$ of sodium (orange) and $n_-(z)$ of chloride (blue) confined within two parallel combined GR-hBN-GR planar surfaces with glide interface. The area of hBN ribbon is $2 \times 8\ nm^2$. Results are shown for different electrolyte concentrations: (a) 0.1 M, (b) 0.5 M, (c) 1.0 M, (d) 2.0 M. For all the systems, two surfaces are located at $z = -h/2$ and $z = h/2$ where $h = 3.4\ nm$.

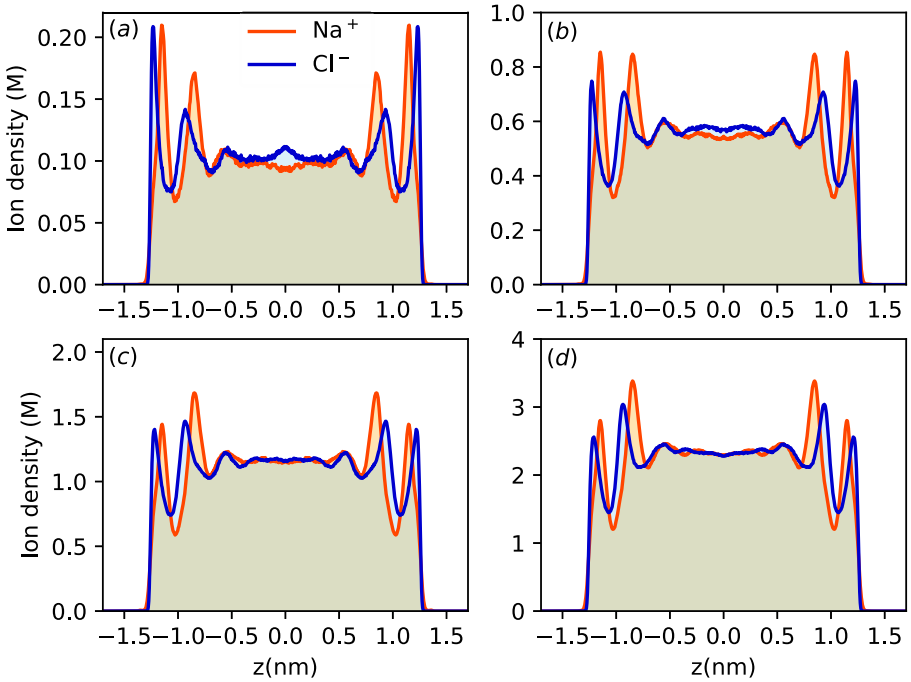

Fig. 6. Density profiles of $n_+(z)$ of sodium (orange) and $n_-(z)$ of chloride (blue) confined within two combined GR-hBN-GR planar surfaces with shuffle interface. The area of hBN ribbon is $2.1 \times 8\ nm^2$. Results are shown for different electrolyte concentrations: (a) 0.1 M, (b) 0.5 M, (c) 1.0 M, (d) 2.0 M. For all the systems, two surfaces are located at $z = -h/2$ and $z = h/2$ where $h = 3.4\ nm$. Notice that in shuffle configuration, the density is much higher than all previous experiments (see Fig. 3–5).

concentration ($c = 0.1M$), the depletion of Cl^- ions from the surface is strong and it is slightly weaker as the salt concentration increases. With increasing salt concentration, the entropic forces between Cl^- ions and the surface become strong and they overcome the repulsive electrostatic forces. As a result, a small layer of Cl^- ions near the hBN surface was observed at higher salt concentration ($2M$). Fig. 5 and Fig. 6 present the density profiles of sodium and chloride ions confined within two combined GR-hBN-GR surfaces with glide and shuffle interfaces respectively. In case of glide interface (Fig. 5), the interface exhibits a weak affinity to Na^+ ions and is repulsive to the Cl^- ions at low salt concentration $c \in (0.1, 0.5)$ M. Increasing the salt concentration $c \in (1, 2)$ M can slightly improve the adsorption capacity of the Cl^- ion at the interface. In the case of shuffle interface (Fig. 6), in all concentrations,

both Na^+ and Cl^- ions have higher accumulation near the GR-hBN-GR surface compared to graphene, hBN and glide GR-hBN-GR surfaces as evidenced by the peaks of $n_+(z)$ and $n_-(z)$. The contact density of chloride ions is slightly closer to the surface (thus experiences a stronger electrostatic attraction) compared to sodium ions. The ion density profiles of similar systems where the area of hBN ribbon is less (1.2×8 nm^2) are shown in the Appendix (see Fig. A.14). These density profiles are not significantly altered by changing the area of hBN ribbon on shuffle GR-hBN-GR surface (similar peak heights, within statistical uncertainty).

From Figs. 3–6, one can conclude that density profiles of ions strongly depend on the surface material, causing the density profiles to be highly specific to the characteristics of the surface and the type of interface between hBN and graphene. To probe the water distribution near these surfaces, the density profiles of O_{water} (z) and electrolyte at 0.5 M concentration confined in two graphene sheets (Fig. 7a), hBN sheets (Fig. 7b) and GR-hBN-GR sheets with glide and shuffle interfaces (Fig. 7c and Fig. 7d respectively) were plotted. All four materials produce a strong layering of water distribution with similar orientational structures near the interfaces [59,60]. The orientational structure of water is also similar in these materials. However, the contact density of water near hBN sheet is higher than graphene and GR-hBN-GR surfaces. Similar equilibrium water structures near graphene and hBN are also observed in *ab initio simulations [36,32], indicating that these force-field parameters for the solid/water interaction are accurately described. As seen in Fig. 7 (c and d), the water density profiles near GR-hBN-GR surface are not significantly altered by varying the type of interfaces.*

Note that the density distribution of ions in the *z*-direction (the direction perpendicular to the surfaces) is an average distribution of ions over all surface areas (*xy* plane). Since GR-hBN-GR surface is not homogeneous like graphene and hBN surfaces, to provide complementary information on how the electrolyte interact with GR-hBN-GR surface with shuffle and glide interfaces (Fig. 8 and Fig. 9 respectively), the ion density profiles for electrolyte at 0.5 M at *z* direction for four separated regions were defined: (i) the region where carbon atoms are connected with boron atoms in hBN-GR junction (see Fig. 8a, and Fig. 9a), (ii) the region where carbon atoms are connected with nitrogen atoms in hBN-GR junction (Fig. 8b and Fig. 9b), (iii) the regions where graphene (Fig. 8c and Fig. 9c) and (iv) hBN (Fig. 8d and Fig. 9d) surfaces are located in GR-hBN-GR surface. Fig. 8a shows that highest peak concentration of Cl^- ions occurs at a position close to the area where carbon atoms are connected with boron atoms in hBN-GR junction across zigzag bonds. On the other hand, the area where carbon atoms are connected with nitrogen atoms in hBN-GR junction attracts maximum Na^+ ions towards it (Fig. 8b). However, accumulation of sodium ions near nitrogen atoms is much less than accumulation of chloride ions near boron atoms in shuffle interfaces.

No significant difference was observed between the ion distribution where the electrolyte is in contact with graphene areas (Fig. 8c) compared to Fig. 3b where the electrolyte is confined between two homogeneous parallel graphene sheets. In Fig. 8d, an increase in density of both Na^+ and Cl^- ions close to the hBN ribbon was observed. This is in contrast with ion density observed for electrolyte at 0.5 *M* confined in homogeneous hBN sheets (see Fig. 4b). Indeed a depletion of chloride ions confined in homogeneous hBN sheets at 0.5 M was observed. In the case of glide interface, a small adsorption of sodium ions is observed near both junctions where boron and nitrogen atoms are connected with carbon atoms as shown in Fig. 9a and Fig. 9b respectively. Chloride ions are depleted near the junction where the nitrogen atoms are connected with carbon atoms (Fig. 9b). The density profiles near graphene and hBN surfaces in GR-hBN-GR heterostructure with glide interface (Fig. 9c and Fig. 9d respectively), are very similar with density profiles shown near homogeneous graphene and hBN surfaces (Fig. 3b and Fig. 4b respectively). From these results one can infer that the molecular interactions between ions and hBN-GR junctions across zigzag bonds play an important role in determining the distribution of ions near the GR-hBN-GR channel wall. The density profiles of hydrogen and oxygen of water molecules at these four regions on GR-hBN-GR surfaces with shuffle and glide interfaces are shown in the Appendix (Fig. A.15 and Fig. A.16 respectively). To examine the ion distributions in parallel to the GR-hBN-GR surfaces, in Fig. 10, the ion density profiles of electrolytes at 0.5 M in *x* direction for three cases are shown: (1) glide interface where the area of hBN ribbon is 2.1×8 nm^2 (see Fig. 10a) (2) shuffle interface where the area of hBN ribbon is 2.1×8 nm^2 (see Fig. 10b) (3) shuffle interface where the area of

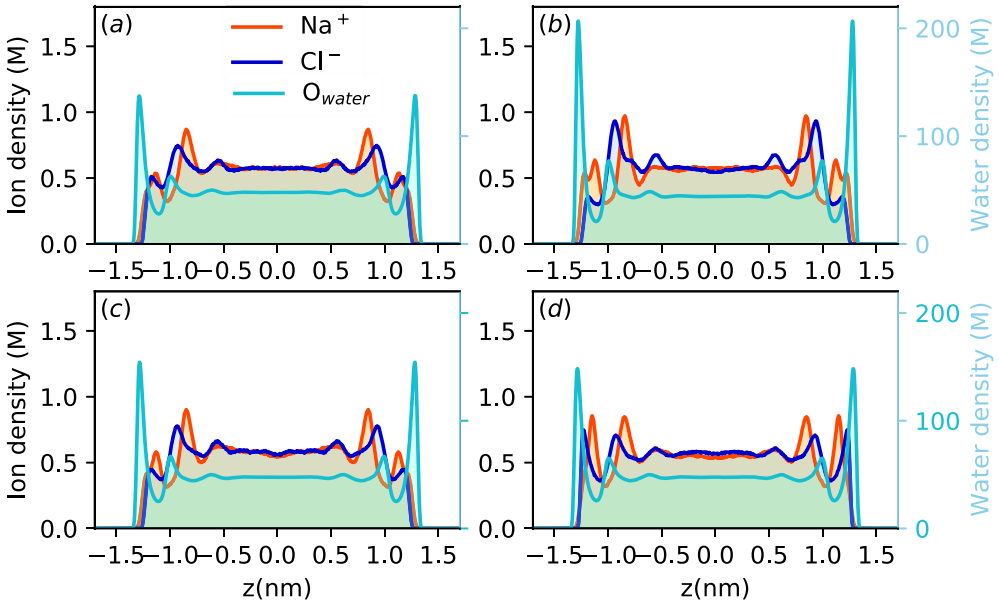

Fig. 7. Density profiles of sodium (orange) and chloride (blue) and O_{water} (cyan) confined in two parallel sheets made of: (a) graphene, (b) hBN, (c) GR-hBN-GR with glide interfaces, (d) GR-hBN-GR with shuffle interfaces. Results are shown for electrolyte with 0.5 M concentration.

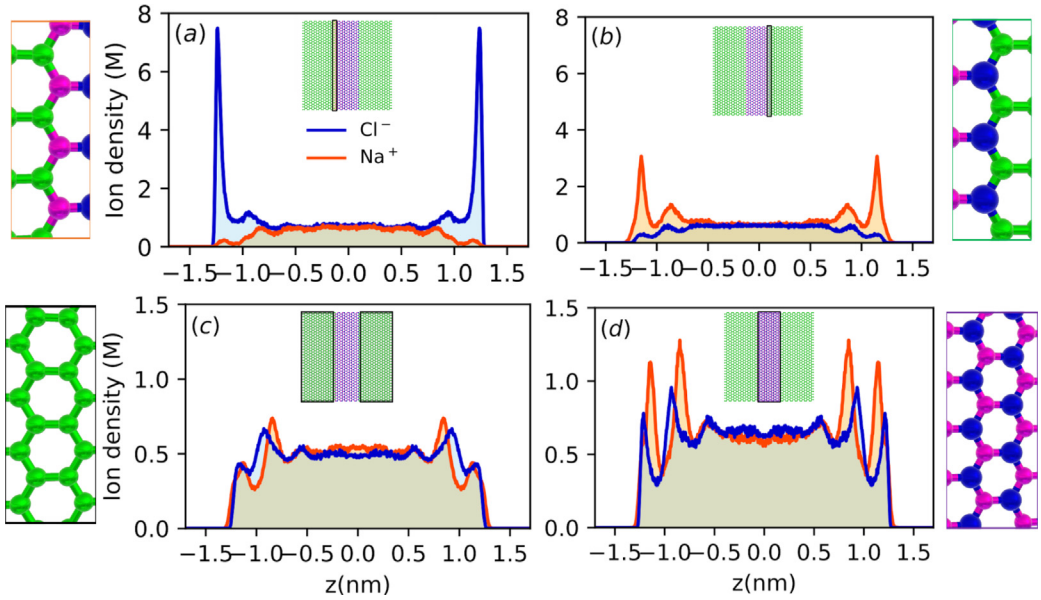

Fig. 8. Density profile $n_+(z)$ of sodium (orange) and $n_-(z)$ of chloride (blue) ions (in z direction) confined within two combined GR-hBN-GR planar surfaces with shuffle interface at different areas: (a) the area where boron and carbon atoms are connected at hBN-GR junction, (b) the area where nitrogen and carbon atoms are connected at hBN-GR junction, (c) the area where graphene is in contact with electrolyte, d) the area where hBN is in contact with electrolyte. Carbon, boron and nitrogen atoms are colored in green, purple and blue respectively.

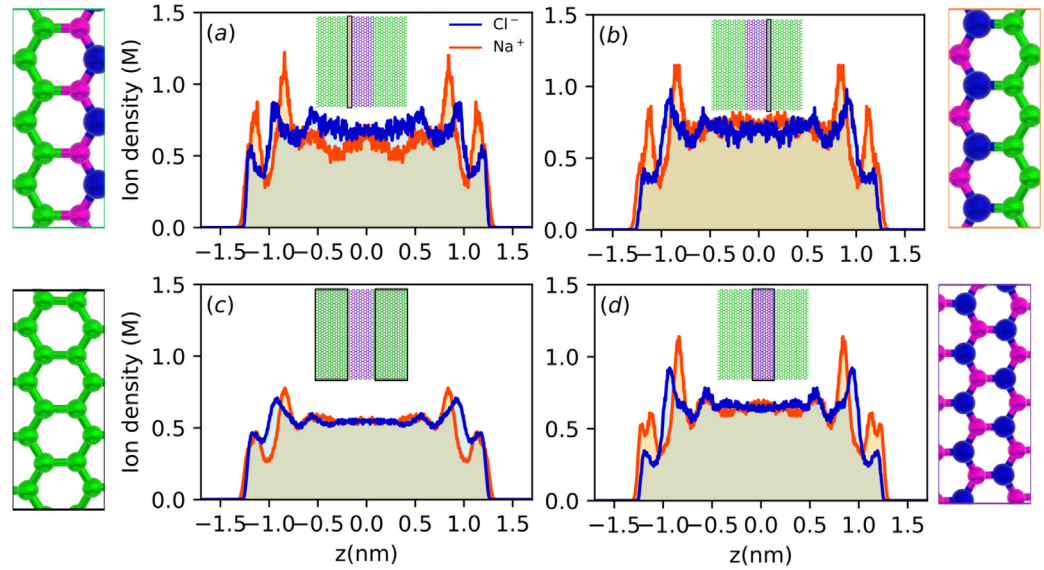

Fig. 9. Density profile $n_+(z)$ of sodium (orange) and $n_-(z)$ of chloride (blue) ions (in z direction) confined within two combined GR-hBN-GR planar surfaces with glide interface at different areas: (a) the area where boron and carbon atoms are connected at hBN-GR junction, (b) the area where nitrogen and carbon atoms are connected at hBN-GR junction, (c) the area where graphene is in contact with electrolyte, d) the area where hBN is in contact with electrolyte. Carbon, boron and nitrogen atoms are colored in green, purple and blue respectively. (For interpretation of the references to colour in this figure legend, the reader is referred to the web version of this article.)

hBN ribbon is 1.2×8 nm^2 (see Fig. 10c). The results shows no significant adsorption of Na^+ and Cl^- ions near glide interfaces (Fig. 10a) while there is a high accumulation of Na^+ and Cl^- ions near the shuffle interfaces (Fig. 10b) up to 2 times higher than bulk concentration. In case of shuffle interface, the height of Na^+ and Cl^- peaks does not change significantly by changing the hBN area from 2.1×8 nm^2 down to 1.2×8 nm^2. But the location of the Na^+ and Cl^- peaks depend on the width of hBN ribbon where the hBN-GR junctions are located. These results are consistent with the quantitative plots shown in Fig. 10 capturing the accumulation of Na^+ and Cl^- ions near the nitrogen and boron atoms respectively.

3.2. Potential of Mean Force (PMF)

In order to have an intuitive impression on the interaction energy profile, the profile of potential of mean force (PMF) was calculate for the sodium and chloride ions (Fig. 11a and Fig. 11b respectively) at c = 0.5 M in these nanochannels. Since the PMF values show symmetry for the given channels, we show the free energy profile for half of the channel height, where an interesting phenomenon occurs close to the wall surface region. The fluctuating manner of the PMF profile corresponds to the reorganization of Na^+ and Cl^- ions in the region among two approaching these

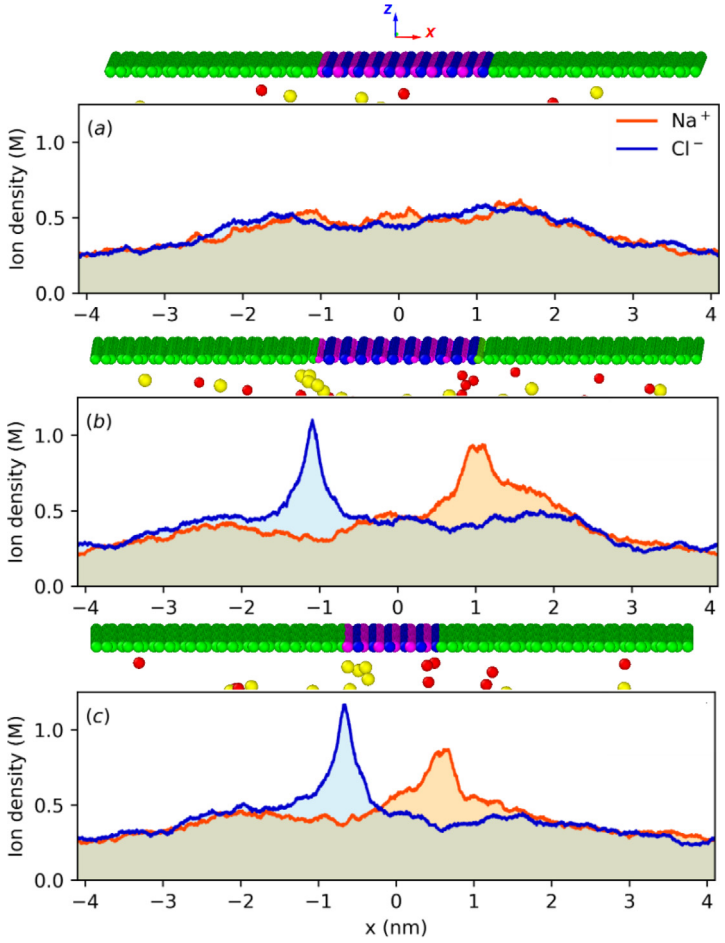

Fig. 10. Density profiles of $n_+(z)$ of sodium (orange) and $n_-(z)$ of chloride (blue) ions (in x direction) confined within two combined GR-hBN-GR planar surfaces. (a) The area of hBN ribbon is 2.1×8 nm^2 with glide interfaces, b) The area of hBN ribbon is 2.1×8 nm^2 with shuffle interfaces. c) The area of hBN ribbon is 1.2×8 nm^2 with shuffle interfaces. Representative snapshots of ions near the surface extracted from the simulations of electrolytes at c = 0.5 M are shown above each plot. Carbon, boron and nitrogen atoms are colored in green, purple and blue respectively. Water is not shown. (For interpretation of the references to colour in this figure legend, the reader is referred to the web version of this article.)

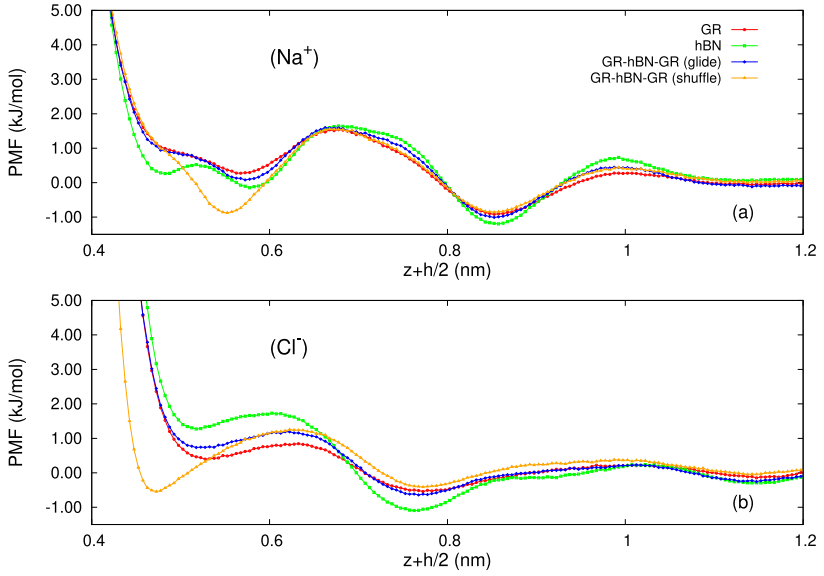

Fig. 11. Potential of mean force (PMF) as a function of the separation between a two graphene surfaces, hBN surfaces, glide GR-hBN-GR surfaces and shuffle GR-hBN-GR surfaces for (a) Na^+ ions and (b) Cl^- ions moving along the z direction. In both figures, the PMF calculated for the electrolytes at c = 0.5 M.

nanochannels. The depth of the first minimum is said to be more energetically favorable [61]. As shown in Fig. 11a, the intense adsorption of sodium ions corresponds to minimum PMF value of $-0.98\ kJ/mol$ at an interfacial distance of 0.55 *nm* near the shuffle GR-hBN-GR surface. The points corresponding to the second minimum potential energy for shuffle GR-hBN-GR surface ($-0.85\ kJ/mol$) have emerged at the 0.83 *nm* distance. Near these nanochannels, much smaller fluctuations continued to 1.1 *nm* and PMF fluctuations tended to zero at distances greater than 1.1 *nm*. Fig. 11b shows near shuffle GR-hBN-GR surface, the Cl^- ions exhibit local minima in PMF at position 0.47 *nm* from the surface and it is shifted to the surface compared to the position of the local minima in PMF for Na^+ ions. As expected, the overall shape of the PMF profiles for both Na^+ and Cl^- ions (Fig. 11a and Fig. 11b respectively) near the glide GR-hBN-GR surfaces are comparable to that of the PMF profiles near the graphene surface. The PMF's overall shape and structure near the glide GR-hBN-GR surface appears to be significantly affected by the graphene region in GR-hBN-GR. From the PMF plots, it is deduced that near the shuffle GR-hBN-GR surface, the first minimum wells for Na^+ and Cl^- ions are the deepest and adsorption is favored compared to other nanochannels.

3.3. Net Charge Density

To explore the dynamics of the charging process, the charge density $\rho(z)$ distribution profiles by employing Eq. 3 were defined. The charge density distribution is derived by summing over the individual charged Na^+ and Cl^- ions, taking into account the charge numbers with their sign. Fig. 12a, Fig. 12b, 12c and 12d show $\rho(z)$ for the same systems explored in Fig. 3, Fig. 4, Fig. 5 and Fig. 6 respectively. $\rho(z)$ is symmetric around the center of the confinement (z = 0). For the ease of exposition, we discuss the behavior of ρ near the left interface. In the immediate vicinity of these surfaces, ρ is positive and exhibits a peak close to the interface that can be attributed to presence of Na^+ ions due the smaller size of Na^+ ion than that of Cl^+ ion. However, the magnitude of positive ρ is different near these surfaces.

Near graphene sheet (Fig. 12a), upon growing ion concentrations, a region close to the first layer develops where ρ becomes negative. Alternating layers of positive/negative net charge appear until the magnitude of the net charge reaches a maximum before charge neutrality is achieved in the middle of the channel. The height of peaks increases with increasing concentration from 0.1 M to 2 M.

Near the hBN surface (Fig. 12b), two sequential positive ρ peaks due to the accumulation of Na^+ ions and depletion of Cl^- ions were observed. This indicated that hBN surface is more favorable for the sodium ions than chloride ions and it is a manifestation of strong electrostatic correlations between the Na^+ ions and the hBN surface. As a result, a negative net charge appears near these positive layers to neutralize the effect of cumulative positive charge density. In the case of hBN surface, the breakdown of charge neutrality and the magnitude of net charge layering are significantly more pronounced as the salt concentration increases. The net charge density gradually goes to zero in the middle of the channel resulting in charge neutrality in that region. The net charge density profiles of electrolytes in vicinity of GR-hBN-GR surfaces with glide and shuffle interfaces are shown in Fig. 12c and Fig. 12d respectively. Similar structure of the net charge density of ions near the glide interface (Fig. 12c) and the homogeneous graphene interface (Fig. 12a) indicates that the ion distribution is mainly governed by the graphene area in GR-hBN-GR surfaces with glide junctions. In case of shuffle interface (Fig. 12d), the first positive layer of ρ near the surface reached its minimum peak and a larger negative ρ appears next to the first layer compared to other surfaces. This can be attributed to the strong accumulation of Cl^- ions near the interface shown in Fig. 6.

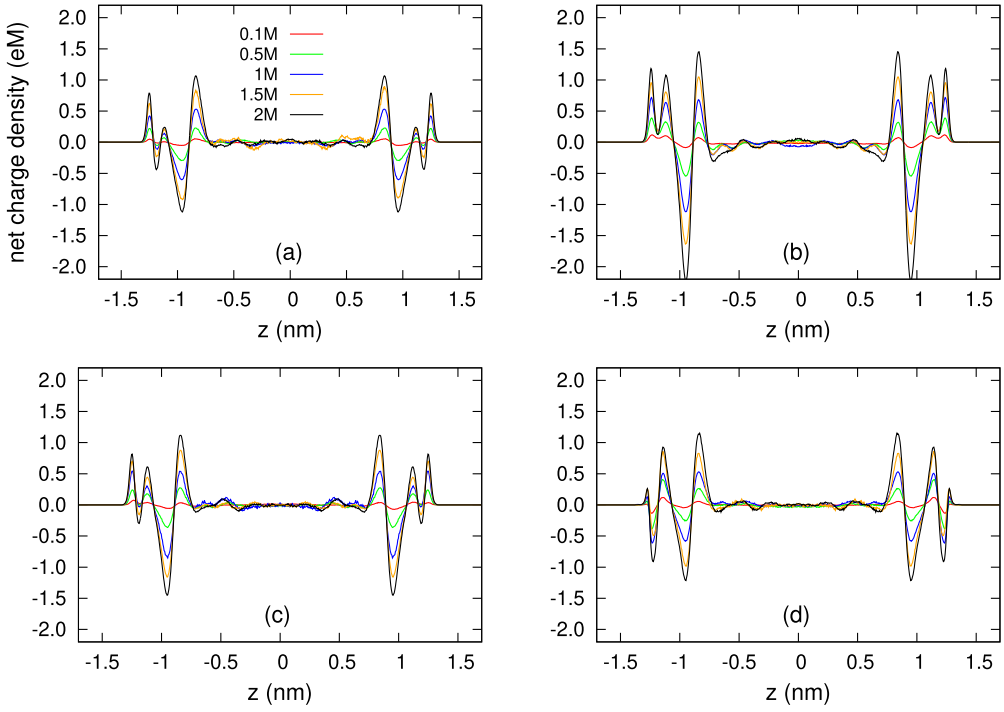

Fig. 12. Net charge density for confined electrolytes under different electrolyte concentrations $c \in (0.1, 2)$ M. Electrolytes are confined by: (a) graphene surfaces, (b) hBN surfaces, (c) glide GR-hBN-GR surfaces, (d) shuffle GR-hBN-GR surfaces. In combined GR-hBN-GR, the hBN ribbon area is $2.1 \times 8\ nm^2$.

3.4. Integrated charge

To reveal the effects of ion depletion or accumulation on electrostatic correlations near the interfaces, Fig. 13 shows the integrated charge (S) of electrolytes near: (a) graphene, (b) hBN, (c) GR-hBN-GR with glide interface and (d) GR-hBN-GR with shuffle interface.

Due to the obvious ionic layered distributions, the integrated charge profile of NaCl shows an oscillatory shape, as shown in Fig. 13. Since the surface charge density of these surfaces is zero, the integrated charge density is zero up to a distance of the closest approach of the sodium ions. Then integrated charge rises to values > 0 and exhibits a non-monotonic, oscillatory decay to 0 for large $z + h/2$. As seen in Fig. 13a, near the graphene surface, integrated charge increased slightly with increasing salt concentration. Of special interest in this work is that our data yield large cumulative positive charge density for cases of electrolytes near the hBN surface (Fig. 13b). Near the hBN surfaces, integrated charge rises remarkably and exhibits more oscillatory behavior. A rapid rise in integrated charge could be due to the absorption of sodium and depletion of chloride near the hBN surfaces (see Fig. 4). As the salt concentration increases, integrated charge continues to rise rapidly to values beyond 0, reaching much higher peaks (e.g., $> 0.14\ C/m^2$ for 2 M). The integrated charge near the GR-hBN-GR surface with glide interface (Fig. 13c) exhibits a similar oscillatory behavior to the integrated charge for the graphene surface (Fig. 13a) with slightly different amplitudes. This can be attributed to the fact that the ion distribution is more affected by the graphene area in GR-hBN-GR surfaces with glide junctions. The integrated charge plot in Fig. 13d shows a very small rise near the GR-hBN-GR surface with shuffle interface. As concentration rises to values 2 M, a prominent negative charge develops adjacent to the first positive peak close to the interface and the minimum value of integrated charge drops slightly. The drop can be attributed to the strong accumulation of chloride ions near the interface shown in Fig. 6.

4. Discussion

All-Atom molecular dynamics simulations were employed to investigate the ionic distribution and adsorption of monovalent NaCl electrolyte from 0.1M to 2M confined by graphene, hBN and GR-hBN-GR nanochannels. The ionic structures were quantified by evaluating the density profiles of ions, PMF, net charge densities, and integrated charges across these channels. The main highlights of the results in the current work are summarized as follows. Despite very similar interface structures in graphene and hBN, significant changes in ion density profiles in the vicinity of these surfaces were found. The results show an enhancement in the sodium accumulation and depletion of chloride ions in immediate contact with the hBN surface compared to the graphene surface. However, as the salt concentration increases, the depletion of Cl^- from the hBN surface weakens. The density profiles of the electrolytes confined in the combined GR-hBN-GR with shuffle interface showed the simultaneous adsorption of Na^+ and Cl^- ions near the surfaces. The results of ion distribution at different regions of GR-hBN-GR surface with shuffle interface showed that the high adsorption of Na^+ and Cl^- ions are due to the electrostatic attractions between the Na^+ and the nitrogen atoms and between Cl^- ions and boron atoms at the hBN-GR junctions across zigzag bonds respectively. Moreover, the accumulation of chloride ions near boron–carbon connection is much more than accumulation of sodium ions near nitrogen-carbon connection in shuffle interfaces. In contrast, the results of ion density profiles near the combined GR-hBN-GR with glide interface show no significant adsorption of Na^+ and Cl^- ions near the hBN-GR junctions across parallel bonds.

The ionic densities for different regions on shuffle GR-hBN-GR surface show that the hBN ribbon is favorable for both the sodium and chloride ions. This is in contrast with the ionic density found near the homogeneous hBN surface. Near the homogeneous structure of hBN, a depletion of chloride ions was observed. The structure and dynamics of water in contact with these four materials

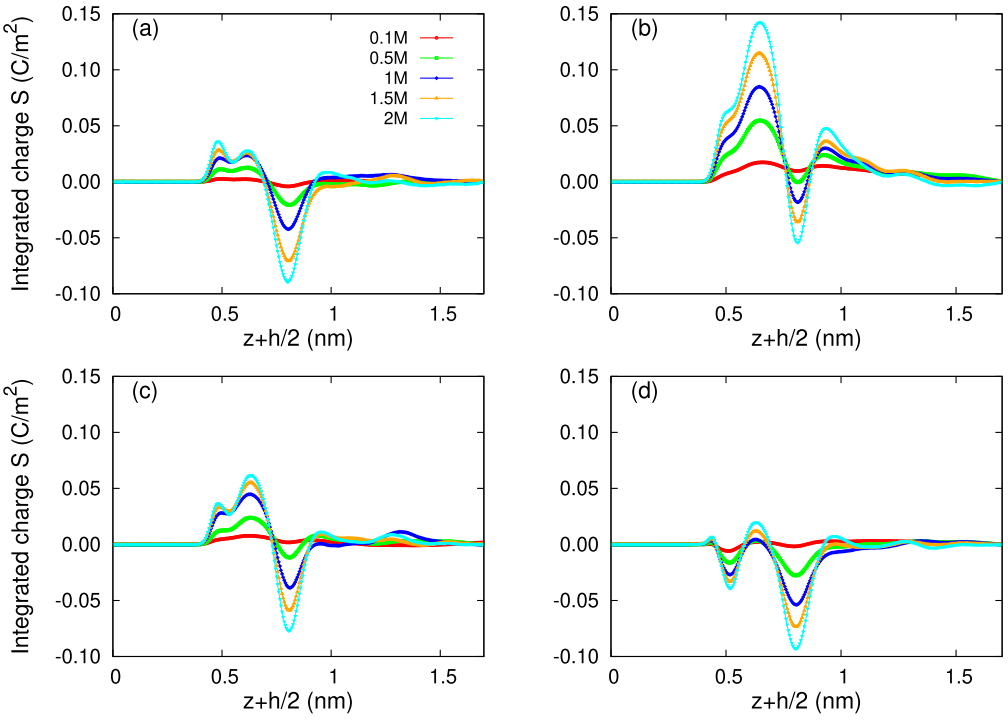

Fig. 13. Integrated charge S(z) vs the distance $z + h/2$ where $h = 3.4\ nm$ from the left interface for electrolytes confined in two: a) graphene surfaces, b) hBN surfaces, c) glide GR-hBN-GR surfaces, d) shuffle GR-hBN-GR surfaces. In combined GR-hBN-GR, the hBN ribbon area is $2.1 \times 8\ nm^2$.

were compared. The results showed similarity between the structure of water in contact with these four materials. Nevertheless, the contact density of water is higher for hBN than GR and GR-hBN-GR surfaces.

From the PMF plots, it is deduced that near the shuffle GR-hBN-GR surface, the first minimum wells for Na^+ and Cl^- ions are the deepest and adsorption is favored compared to other nanochannels. A positive net charge density of the electrolyte near all studied surfaces was observed. However, the oscillatory nature of the charge density and its magnitude are different near these surfaces. Upon growing ion concentrations, structural profiles of net charge near the hBN surface display a stronger oscillation over a longer range. The reason lies in that ion-ion correlations near the hBN surface require travelling a longer distance so that the system can return back to bulk state. The oscillatory nature of the charge density makes the integrated charge non-monotonic near these four surfaces (see Fig. 13). A concentration-dependent scaling behavior of the integrated charge of electrolytes near these interfaces is reported. As the salt concentration increases, the simulations reveal a significant cumulative positive charge density near the hBN surface due to the adsorption of sodium and the depletion in chloride density. These results provide insights into the electrostatically driven ion adsorption of confined electrolytes in graphene, hBN and combined GR-hBN-GR surfaces and thus have important implications for the utilization of electrolytes in numerous applications, including artificial ionic channels, electrochemical storage devices and self-assembly media.

5. Conclusion

The current study provides an account of the nature of interactions and dynamics between the confined water and electrolytes near graphene, hBN and their heterostructures. It was found that GR-hBN-GR with shuffle interface is significantly more advantageous in simultaneously adsorbing sodium and chloride ions than GR-hBN-GR with glide interface. The ionic structure of electrolytes near the homogeneous hBN surface is different from the hBN ribbon located in the shuffle GR-hBN-GR surface. Furthermore, graphene and hBN nanomaterials are noncytotoxic to proteins and cells as reported in [62,63], therefore our findings can be used to synthesize biological interfaces. In addition, such systems are highly useful in quantum electronics as reported in [64].

Although, most Gr-hBN-Gr experiments [65] use glide interface, our results clearly demonstrate that the use of shuffle interfaces can significantly absorb more ions. Therefore, we highly recommend synthesizing shuffle interfaces for effective and advanced product development.

Declaration of Competing Interest

The authors declare that they have no known competing financial interests or personal relationships that could have appeared to influence the work reported in this paper.

Appendix A. Supplementary Results

Fig. A.14 shows the density profiles of sodium and chloride ions confined within two combined GR-hBN-GR surfaces with shuffle interface in the z direction. The area of the hBN ribbon in GR-hBN-GR surface is 1.2 $\times$ 8 nm^2. These density profiles are very similar with ion density profiles near GR-hBN-GR surface when area of the hBN ribbon is 2.1 $\times$ 8 nm^2 (see Fig. 6). This indicates that the width of hBN ribbon in GR-hBN-GR surface does not change the ion density significantly and the shuffle interface between the GR-hBN plays an important role on determination of ion distribution near GR-hBN-GR surface.

The density profiles of hydrogen and oxygen of water molecules at four regions on GR-hBN-GR surfaces with shuffle and glide interfaces are shown in Fig. A.15 and Fig. A.16 respectively. In case of shuffle, the maximum adsorption of water molecules is seen near the boron–carbon connection (Fig. A.15a). Near the nitrogen-carbon connection, there is a tendency for some of the O-H bonds

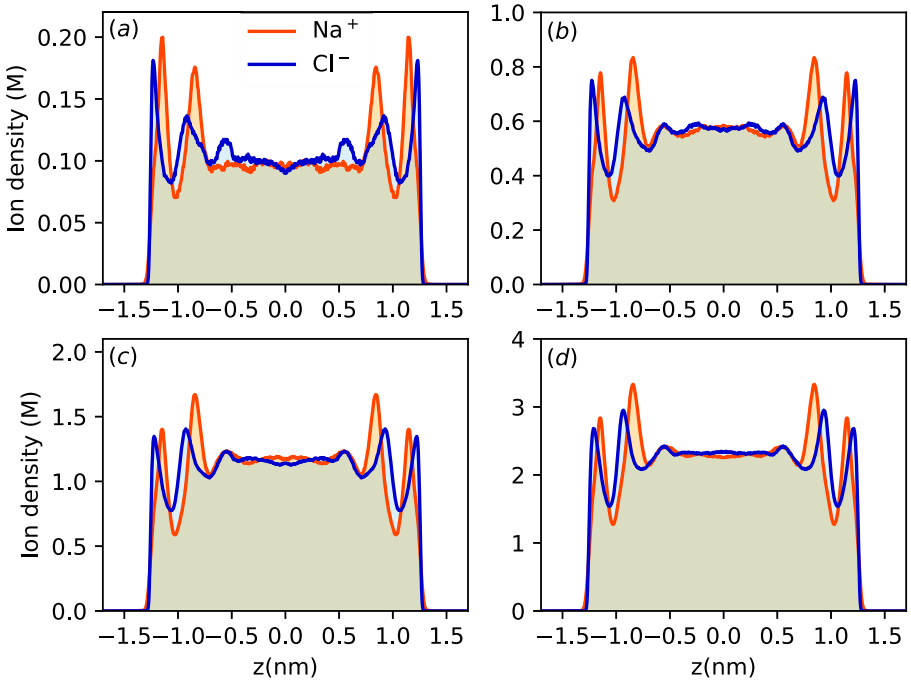

Fig. A.14. Density profiles of $n_+(z)$ of sodium (orange) and $n_-(z)$ of chloride (blue) confined within two combined GR-hBN-GR planar surfaces with shuffle interface. The area of hBN ribbon is 1.2 $\times$ 8 nm^2. Results are shown for different electrolyte concentrations: (a) 0.1 M, (b) 0.5 M, (c) 1.0 M, (d) 2.0 M. For all the systems, two surfaces are located at $z = -h/2$ and $z = h/2$ where h = 3.4 nm.

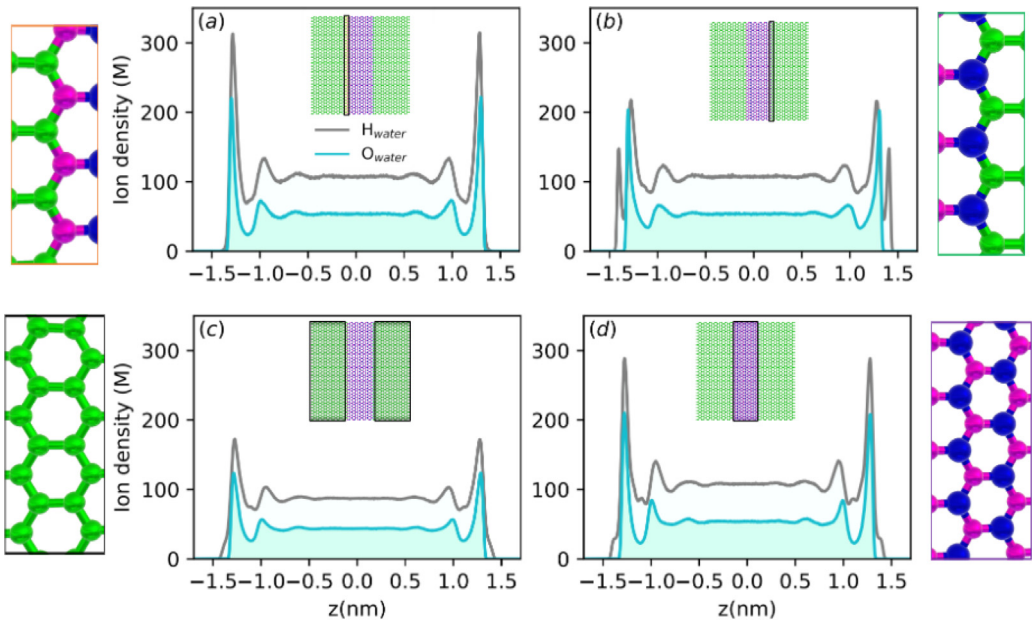

Fig. A.15. Density profiles of $O_{water}(z)$ (cyan) and $H_{water}(z)$ (gray) of water molecules in z direction confined within two combined GR-hBN-GR planar surfaces with shuffle interface at different areas: (a) the area where boron and carbon atoms are connected at hBN/graphene junction (b) The area where nitrogen and carbon atoms are connected at hBN/graphene junction, (c) the area where graphene is in contact with electrolyte, (d) the area where hBN is in contact with electrolyte. Carbon, boron and nitrogen atoms are colored in green, purple and blue respectively. The electrolyte concentration is 0.5 M.

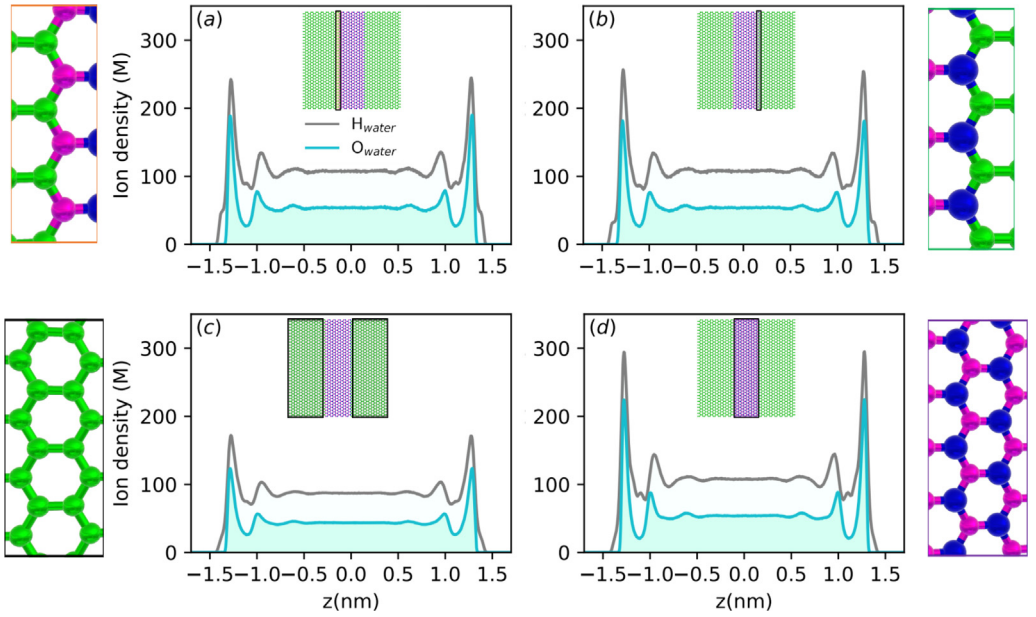

Fig. A.16. Density profiles of $O_{water}(z)$ (cyan) and $H_{water}(z)$ (gray) of water molecules in z direction confined within two combined GR-hBN-GR planar surfaces with glide interface at different areas: (a) the area where boron and carbon atoms are connected at hBN/graphene junction (b) The area where nitrogen and carbon atoms are connected at hBN/graphene junction, (c) the area where graphene is in contact with electrolyte, (d) the area where hBN is in contact with electrolyte. Carbon, boron and nitrogen atoms are colored in green, purple and blue respectively. The electrolyte concentration is 0.5 M.

to arrange themselves such that the hydrogen atoms are oriented towards the negatively charged nitrogen centers. As a result, the layer of hydrogen preferentially oriented towards the nitrogen center near this region was found (see Fig. A.15b). Near graphene (Fig. A.15c), the lowest adsorption of water was observed. Many experiments [66,67] and simulations [68,69] studies have shown that graphene behaves like a hydrophobic surface that leads to weak wettability of the graphene surface. As shown in Fig. A.16, the molecular orientation of water molecules near the four regions in GR-hBN-GR with parallel junctions are similar. However, the contact density of water molecules near the region where hBN is in contact is higher than other regions.

References

[1] A. Boretti, S. Al-Zubaidy, M. Vaclavikova, M. Al-Abri, S. Castelletto, S. Mikhalovsky, Outlook for graphene-based desalination membranes, npj Clean Water 1 (1) (2018) 1–11.

[2] M. Aminpour, C. Montemagno, J.A. Tuszynski, An overview of molecular modeling for drug discovery with specific illustrative examples of applications, Molecules 24 (9) (2019) 1693.
[3] L. Feng, Z. Liu, Graphene in biomedicine: opportunities and challenges, Nanomedicine 6 (2) (2011) 317–324.
[4] X. Zhou, F. Liang, Application of graphene/graphene oxide in biomedicine and biotechnology, Curr. Med. Chem. 21 (7) (2014) 855–869.
[5] L. Xue, B. Lu, Z.-S. Wu, C. Ge, P. Wang, R. Zhang, X.-D. Zhang, Synthesis of mesoporous hexagonal boron nitride fibers with high surface area for efficient removal of organic pollutants, Chem. Eng. J. 243 (2014) 494–499.
[6] M. Li, W. Zhu, P. Zhang, Y. Chao, Q. He, B. Yang, H. Li, A. Borisevich, S. Dai, Graphene-analogues boron nitride nanosheets confining ionic liquids: A high-performance quasi-liquid solid electrolyte, Small 12 (26) (2016) 3535–3542.
[7] Z. Liu, L. Ma, G. Shi, W. Zhou, Y. Gong, S. Lei, X. Yang, J. Zhang, J. Yu, K.P. Hackenberg, et al., In-plane heterostructures of graphene and hexagonal boron nitride with controlled domain sizes, Nature nanotechnology 8 (2) (2013) 119–124.
[8] L. Liu, J. Park, D.A. Siegel, K.F. McCarty, K.W. Clark, W. Deng, L. Basile, J.C. Idrobo, A.-P. Li, G. Gu, Heteroepitaxial growth of two-dimensional hexagonal boron nitride templated by graphene edges, Science 343 (6167) (2014) 163–167.
[9] N. Hasan, B. Hou, A.L. Moore, A.D. Radadia, Enhanced ionic sensitivity in solution-gated graphene-hexagonal boron nitride heterostructure field-effect transistors, Advanced Materials Technologies 3 (8) (2018) 1800133.
[10] C.R. Dean, A.F. Young, I. Meric, C. Lee, L. Wang, S. Sorgenfrei, K. Watanabe, T. Taniguchi, P. Kim, K.L. Shepard, et al., Boron nitride substrates for high-quality graphene electronics, Nature nanotechnology 5 (10) (2010) 722–726.
[11] M.-K. Hong, S.-H. Hyun, H.-S. Jang, B.-S. An, H.-C. Jang, H.-S. Hwang, S.-I. Kim, J.-Y. Moon, S.M. Sattari-Esfahlan, S.-Y. Lee, et al., Controlled growth of in-plane graphene/h-bn heterostructure on a single crystal ge substrate, Appl. Surf. Sci. 554 (2021) 149655.
[12] H.S. Wang, L. Chen, K. Elibol, L. He, H. Wang, C. Chen, C. Jiang, C. Li, T. Wu, C.X. Cong, et al., Towards chirality control of graphene nanoribbons embedded in hexagonal boron nitride, Nat. Mater. 20 (2) (2021) 202–207.
[13] M. Xu, D. Fujita, N. Hanagata, Perspectives and challenges of emerging single-molecule dna sequencing technologies, Small 5 (23) (2009) 2638–2649.
[14] Z. He, R. Zhou, Exploring an in-plane graphene and hexagonal boron nitride array for separation of single nucleotides, ACS nano 15 (7) (2021) 11704–11710.
[15] L. Chen, G. Shi, J. Shen, B. Peng, B. Zhang, Y. Wang, F. Bian, J. Wang, D. Li, Z. Qian, et al., Ion sieving in graphene oxide membranes via cationic control of interlayer spacing, Nature 550 (7676) (2017) 380–383.
[16] C. Cheng, J. Uhe, X. Yang, Y. Wu, D. Li, Multilayered graphene membrane as an experimental platform to probe nano-confined electrosorption, Progress in Natural Science: Materials International 22 (6) (2012) 668–672.
[17] J. Abraham, K.S. Vasu, C.D. Williams, K. Gopinadhan, Y. Su, C.T. Cherian, J. Dix, E. Prestat, S.J. Haigh, I.V. Grigorieva, et al., Tunable sieving of ions using graphene oxide membranes, Nature nanotechnology 12 (6) (2017) 546–550.
[18] A. Gubbiotti, M. Baldelli, G. Di Muccio, P. Malgaretti, S. Marbach, M. Chinappi, Electroosmosis in nanopores: Computational methods and technological applications, arXiv preprint arXiv:2111.05786 (2021).
[19] D.J. Cole, P.K. Ang, K.P. Loh, Ion adsorption at the graphene/electrolyte interface, The Journal of Physical Chemistry Letters 2 (14) (2011) 1799–1803.
[20] H. Zhu, Y. Wang, Y. Fan, J. Xu, C. Yang, Structure and transport properties of water and hydrated ions in nano-confined channels, Advanced Theory and Simulations 2 (6) (2019) 1900016.
[21] L. Sun, X. He, J. Lu, Super square carbon nanotube network: a new promising water desalination membrane, npj Computational Materials 2 (1) (2016) 1–7.
[22] X. Jiang, C. Zhao, Y. Noh, Y. Xu, Y. Chen, F. Chen, L. Ma, W. Ren, N.R. Aluru, J. Feng, Nonlinear electrohydrodynamic ion transport in graphene nanopores, Science Advances 8 (2) (2022) eabj2510.
[23] A. Ghoufi, P. Malfreyt, Interfacial tension of the graphene–water solid–liquid interface: how to handle the electrostatic interactions?, Mol Phys. 119 (19–20) (2021) e1948121.
[24] G. Lei, D. Chen, X. Zhang, H. Liu, Improving water desalination via inhomogeneous distribution of [bmim][bf4] in 2d carbon nanotube networks: Nonequilibrium molecular dynamics simulation, J. Mol. Liq. 331 (2021) 115813.
[25] D. Cohen-Tanugi, J.C. Grossman, Water desalination across nanoporous graphene, Nano letters 12 (7) (2012) 3602–3608.
[26] C.T. Nguyen, A. Beskok, Water desalination performance of h-bn and optimized charged graphene membranes, Microfluid. Nanofluid. 24 (5) (2020) 1–12.
[27] Z. Cao, G. Markey, A. Barati Farimani, Ozark graphene nanopore for efficient water desalination, J. Phys. Chem. B 125 (40) (2021) 11256–11263.
[28] A.R. Finney, I.J. McPherson, P.R. Unwin, M. Salvalaglio, Electrochemistry, ion adsorption and dynamics in the double layer: a study of nacl (aq) on graphite, Chemical science 12 (33) (2021) 11166–11180.
[29] C.Y. Won, N. Aluru, Water permeation through a subnanometer boron nitride nanotube, J. Am. Chem. Soc. 129 (10) (2007) 2748–2749.
[30] C.Y. Won, N. Aluru, A chloride ion-selective boron nitride nanotube, Chem. Phys. Lett. 478 (4–6) (2009) 185–190.
[31] R. Srivastava, A. Kommu, N. Sinha, J. Singh, Removal of arsenic ions using hexagonal boron nitride and graphene nanosheets: a molecular dynamics study, Mol. Simul. 43 (13–16) (2017) 985–996.
[32] A. Kayal, A. Chandra, Water in confinement between nanowalls: Results for hexagonal boron nitride versus graphene sheets from ab initio molecular dynamics, The Journal of Physical Chemistry C 123 (10) (2019) 6130–6140.
[33] H. Yang, Z. Bo, J. Yan, K. Cen, Influence of wettability on the electrolyte electrosorption within graphene-like nonconfined and confined space, Int. J. Heat Mass Transf. 133 (2019) 416–425.
[34] B. Moeremans, H.-W. Cheng, Q. Hu, H.F. Garces, N.P. Padture, F.U. Renner, M. Valtiner, Lithium-ion battery electrolyte mobility at nano-confined graphene interfaces, Nature communications 7 (1) (2016) 1–7.
[35] A.R. Poggioli, D.T. Limmer, Distinct chemistries explain decoupling of slip and wettability in atomically smooth aqueous interfaces, The journal of physical chemistry letters 12 (37) (2021) 9060–9067.
[36] G. Tocci, L. Joly, A. Michaelides, Friction of water on graphene and hexagonal boron nitride from ab initio methods: very different slippage despite very similar interface structures, Nano letters 14 (12) (2014) 6872–6877.
[37] M. Caglar, I. Silkina, B.T. Brown, A.L. Thorneywork, O.J. Burton, V. Babenko, S.M. Gilbert, A. Zettl, S. Hofmann, U.F. Keyser, Tunable anion-selective transport through monolayer graphene and hexagonal boron nitride, ACS nano 14 (3) (2019) 2729–2738.
[38] R. Drost, A. Uppstu, F. Schulz, S.K. Hamalainen, M. Ervasti, A. Harju, P. Liljeroth, Electronic states at the graphene–hexagonal boron nitride zigzag interface, Nano letters 14 (9) (2014) 5128–5132.
[39] J. Pan, W. Wei, Z. Gong, Y. Cui, Effect of overlayer–substrate interaction on the coalescence behaviors of in-plane graphene/hexagonal boron nitride heterostructures, Carbon 177 (2021) 19–25.
[40] C. Leon, M. Costa, L. Chico, A. Latgé, Interface effects in hybrid hbn-graphene nanoribbons, Scientific reports 9 (1) (2019) 1–11.
[41] S.A. Hollingsworth, R.O. Dror, Molecular dynamics simulation for all, Neuron 99 (6) (2018) 1129–1143.
[42] Y. Wang, C. Wang, Y. Zhang, F. Huo, H. He, S. Zhang, Molecular insights into the regulatable interfacial property and flow behavior of confined ionic liquids in graphene nanochannels, Small 15 (29) (2019) 1804508.
[43] S. Chung, J.H. Lee, M.-W. Moon, J. Han, R.D. Kamm, Non-lithographic wrinkle nanochannels for protein preconcentration, Adv. Mater. 20 (16) (2008) 3011–3016.
[44] J.G. McHugh, P. Mouratidis, A. Impellizzeri, K. Jolley, D. Erbahar, C.P. Ewels, Prismatic edge dislocations in graphite, Carbon 188 (2022) 401–419.
[45] V. Solozhenko, G. Will, F. Elf, Isothermal compression of hexagonal graphite-like boron nitride up to 12 gpa, Solid state communications 96 (1) (1995) 1–3.
[46] N. Ooi, A. Rairkar, J.B. Adams, Density functional study of graphite bulk and surface properties, Carbon 44 (2) (2006) 231–242.
[47] E. Garyfallidis, S. Koudoro, J. Guaje, M.-A. Côté, S. Biswas, D. Reagan, N. Anousheh, F. Silva, G. Fox, F. Contributors, Fury: advanced scientific visualization, Journal of Open Source Software 6 (64) (2021) 3384.
[48] N. Anousheh, S. Koudoro, J. Guaje, E. Garyfallidis, Furious atoms software, https://furiousatoms.com.
[49] K. Kadupitiya, N. Anousheh, S. Marru, G. Fox, V. Jadhao, Ions in nanoconfinement, URL: https://nanohub. org/resources/nanoconfinement, doi: doi 10 (2017).
[50] H. Berendsen, J. Grigera, T. Straatsma, The missing term in effective pair potentials, J. Phys. Chem. 91 (24) (1987) 6269–6271.
[51] B. Luan, R. Zhou, Spontaneous ssdna stretching on graphene and hexagonal boron nitride in plane heterostructures, Nature communications 10 (1) (2019) 1–6.
[52] K. Barros, D. Sinkovits, E. Luijten, Efficient and accurate simulation of dynamic dielectric objects, The Journal of chemical physics 140 (6) (2014) 064903.
[53] S. Plimpton, Fast parallel algorithms for short-range molecular dynamics, Journal of computational physics 117 (1) (1995) 1–19.
[54] S. Nosé, A unified formulation of the constant temperature molecular dynamics methods, The Journal of chemical physics 81 (1) (1984) 511–519.
[55] M. Deserno, C. Holm, How to mesh up ewald sums. i. a theoretical and numerical comparison of various particle mesh routines, The Journal of chemical physics 109 (18) (1998) 7678–7693.
[56] N. Anousheh, F.J. Solis, V. Jadhao, Ionic structure and decay length in highly concentrated confined electrolytes, AIP Advances 10 (12) (2020) 125312.
[57] J. Kadupitiya, N. Anousheh, V. Jadhao, Designing machine learning surrogates using outputs of molecular dynamics simulations as soft labels, arXiv preprint arXiv:2110.14714 (2021).
[58] G. Zuo, R. Shen, S. Ma, W. Guo, Transport properties of single-file water molecules inside a carbon nanotube biomimicking water channel, Acs Nano 4 (1) (2010) 205–210.
[59] D.L. McCaffrey, S.C. Nguyen, S.J. Cox, H. Weller, A.P. Alivisatos, P.L. Geissler, R.J. Saykally, Mechanism of ion adsorption to aqueous interfaces: Graphene/water vs. air/water, Proceedings of the National Academy of Sciences 114 (51) (2017) 13369–13373.
[60] S.E. Strong, J.D. Eaves, Atomistic hydrodynamics and the dynamical hydrophobic effect in porous graphene, The journal of physical chemistry letters 7 (10) (2016) 1907–1912.
[61] M. Forsyth, V. Payne, M. Ratner, S. De Leeuw, D. Shriver, Molecular dynamics simulations of highly concentrated salt solutions: Structural and transport effects in polymer electrolytes, Solid State Ionics 53 (1992) 1011–1026.
[62] X. Chen, P. Wu, M. Rousseas, D. Okawa, Z. Gartner, A. Zettl, C.R. Bertozzi, Boron nitride nanotubes are noncytotoxic and can be functionalized for interaction with proteins and cells, J. Am. Chem. Soc. 131 (3) (2009) 890–891.

[63] G.H. Han, J.A. Rodríguez-Manzo, C.-W. Lee, N.J. Kybert, M.B. Lerner, Z.J. Qi, E.N. Dattoli, A.M. Rappe, M. Drndic, A.C. Johnson, Continuous growth of hexagonal graphene and boron nitride in-plane heterostructures by atmospheric pressure chemical vapor deposition, Acs Nano 7 (11) (2013) 10129–10138.
[64] D. Rodan-Legrain, Y. Cao, J.M. Park, S.C. de la Barrera, M.T. Randeria, K. Watanabe, T. Taniguchi, P. Jarillo-Herrero, Highly tunable junctions and non-local josephson effect in magic-angle graphene tunnelling devices, Nat. Nanotechnol. 16 (7) (2021) 769–775.
[65] J. Park, J. Lee, L. Liu, K.W. Clark, C. Durand, C. Park, B.G. Sumpter, A.P. Baddorf, A. Mohsin, M. Yoon, et al., Spatially resolved one-dimensional boundary states in graphene–hexagonal boron nitride planar heterostructures, Nature communications 5 (1) (2014) 1–6.
[66] G. Hong, Y. Han, T.M. Schutzius, Y. Wang, Y. Pan, M. Hu, J. Jie, C.S. Sharma, U. Muller, D. Poulikakos, On the mechanism of hydrophilicity of graphene, Nano letters 16 (7) (2016) 4447–4453.
[67] C.-J. Shih, Q.H. Wang, S. Lin, K.-C. Park, Z. Jin, M.S. Strano, D. Blankschtein, Erratum: Breakdown in the wetting transparency of graphene [phys. rev. lett. 109, 176101 (2012)], Physical Review Letters 115 (4) (2015) 049901.
[68] T. Werder, J.H. Walther, R. Jaffe, T. Halicioglu, P. Koumoutsakos, On the water-carbon interaction for use in molecular dynamics simulations of graphite and carbon nanotubes, J. Phys. Chem. B 107 (6) (2003) 1345–1352.
[69] H. Li, X.C. Zeng, Wetting and interfacial properties of water nanodroplets in contact with graphene and monolayer boron–nitride sheets, ACS nano 6 (3) (2012) 2401–2409.